





# Coherent photo-thermal noise cancellation in a dual-wavelength optical cavity for narrow-linewidth laser frequency stabilisation

FABIAN DAWEL,<sup>1,2,\*</sup>  ALEXANDER WILZEWSKI,<sup>1,2</sup> SOFIA HERBERS,<sup>1</sup>  LENNART PELZER,<sup>1,2</sup> JOHANNES KRAMER,<sup>1,2</sup> MAREK B. HILD,<sup>1,2</sup> KAI DIETZE,<sup>1,2</sup> LUDWIG KRINNER,<sup>1,2</sup> NICOLAS C. H. SPETHMANN,<sup>1</sup> AND PIET O. SCHMIDT<sup>1,2</sup> 

<sup>1</sup>Physikalisch-Technische Bundesanstalt, Bundesallee 100, 38116 Braunschweig, Germany

<sup>2</sup>Institut für Quantenoptik, Leibniz Universität Hannover, Welfengarten 1, 30167 Hannover, Germany

\*Fabian.Dawel@ptb.de

**Abstract:** Optical resonators are used for the realisation of ultra-stable frequency lasers. The use of high reflectivity multi-band coatings allows the frequency locking of several lasers of different wavelengths to a single cavity. While the noise processes for single wavelength cavities are well known, the correlation caused by multi-stack coatings has as yet not been analysed experimentally. In our work, we stabilise the frequency of a 729 nm and a 1069 nm laser to one mirror pair and determine the residual-amplitude modulation (RAM) and photo-thermal noise (PTN). We find correlations in PTN between the two lasers and observe coherent cancellation of PTN for the 1069 nm coating. We show that the fractional frequency instability of the 729 nm laser is limited by RAM at  $1 \times 10^{-14}$ . The instability of the 1069 nm laser is at  $3 \times 10^{-15}$  close to the thermal noise limit of  $1.5 \times 10^{-15}$ .

Published by Optica Publishing Group under the terms of the [Creative Commons Attribution 4.0 License](https://creativecommons.org/licenses/by/4.0/). Further distribution of this work must maintain attribution to the author(s) and the published article's title, journal citation, and DOI.

## 1. Introduction

Optical Fabry-Pérot cavities are an indispensable tool in precision experiments like gravitational wave detectors [1–3], opto-mechanical systems [4–6], micro-cavities [7,8], or optical atomic clocks [9]. Nowadays, the best optical cavities used for optical clocks reach a fractional length instability of  $4 \times 10^{-17}$  at 1 s [10]. This instability is limited by the thermal noise of the mirror coating. It has been proposed to reduce coating thermal noise by employing different materials and coating stacks [11–14], and this was experimentally demonstrated by introducing aSi into a highly reflective SiO<sub>2</sub>/Ta<sub>2</sub>O<sub>5</sub> coating [15].

Apart from laboratory experiments in well-controlled environments, a rising number of transportable optical clocks [16–23] also have clock laser stabilisation cavities with instabilities below  $1.6 \times 10^{-16}$  at 1 s [24]. Additionally, there are cavity designs for space applications [25–28] requiring even smaller, lighter and more robust setups.

A growing number of spectroscopy experiments use multiple atomic species. The second species is used for sympathetic sideband cooling on a narrow optical transition [29–33] or readout via quantum logic [16,34–37]. Therefore, the demand for stabilising multiple narrow-linewidth lasers by means of an optical cavity is increasing. Separate resonators for each wavelength are expensive and increase the footprint of the experiment, which is a challenge for various applications, such as transportable setups or space applications. One solution is to use highly reflective dual wavelength coating resonators.

Locking multiple lasers to one cavity with one mirror pair has been demonstrated in the past. Different groups locked multiple lasers for Doppler cooling and repumping on the same mirror

pair, to reduce the experimental footprint [38,39] and to compensate for thermal drifts [40]. Multi-wavelength coatings are also often used in transfer-cavity approaches [41–51].

In this work we present to our knowledge for the first time the stabilisation of two lasers to a single narrow-linewidth cavity, using a dual-wavelength coating for 1069 nm and 729 nm and analyse their frequency instability. The photo-thermal effect [24,52–58] was measured in order to estimate the resulting frequency instability caused by optical power fluctuations on the mirrors. In addition, the residual-amplitude modulation (RAM) [59–62] in the setup was characterised. In the present analysis, we focus on the correlation effects caused by the cavity on both lasers. For comparison, we performed measurements of the individual lasers with the other physically blocked. Coherent cancellation effects of the thermal noise between the different coating stacks were observed and characterised.

## 2. Experimental setup

In this experiment we used a 50 mm long, cubic, ultra-low expansion (ULE) glass spacer [63]. The mirror substrates with 0.5" diameter were made from ULE glass. One mirror is flat while the other has a radius of curvature of  $R_2 = 500$  mm. The non-reflective side of each mirror is wedged ( $0.5^\circ$ ) to prevent etalons. The quarter-wave stacks of the coating for the 1069 nm light are on the substrate, with the 729 nm coating stack on top. The coating order was chosen such as to minimise the absorption losses in the coatings and maximise the transmission of the 729 nm light. High transmission is important for (self-)injection-locking a slave diode to the cavity-filtered light in order to improve spectral purity [64–68]. The coating stacks (Made by Layertec) were made of  $\text{SiO}_2$  and  $\text{Nb}_2\text{O}_5$ . The finesse was measured via a ring-down measurement. This resulted in a finesse of 67.2 k and 50.1 k for the 1069 nm and 729 nm cavities, respectively. For this cavity the main contribution to the thermal noise limit is given by the mirror substrate, where the main limitation for times between 0.01 s to 10 s is from Brownian noise. The calculated instability flicker frequency floor for the 729 nm frequency instability was  $\text{mod } \sigma_y = 1.5 \times 10^{-15}$  using the method shown in [69]. The thermal noise limit for the 1069 nm cavity is around 20% lower than the 729 nm thermal noise floor, when only the 1069 nm coating is considered. The difference in coating thickness has only a small impact since it is not the main contributor to the thermal noise limit. The power spectral density of the substrate's thermal noise of the 1069 nm cavity is 2 (3) times larger than the coating thermal noise when the whole (only the 1069 nm) coating stack contributes to the Brownian noise. In the plots presented below, we always show the fractional frequency fluctuations of the 729 nm thermal noise limit.

The estimated frequency shift from acceleration is below the thermal-noise limit for typical laboratory environments. This is achieved by mounting the spacer via four edges of the cube to obtain high mounting symmetry [63]. The measured sensitivity to accelerations at 10 Hz acceleration modulation is:  $\sigma_x = 2.8(6) \times 10^{-11}/\text{g}$ ,  $\sigma_y = 6.9(3) \times 10^{-11}/\text{g}$  and  $\sigma_z = 7.7(5) \times 10^{-11}/\text{g}$ . In principle, insensitivities on the order of  $10^{-12}/\text{g}$  should be feasible with this spacer for two of the three directions, as shown in previous work [63]. For additional vibrational decoupling of the cavity, it was placed on an active vibration isolation platform (Tablestabe, AVI600-M). With the given sensitivity, we reach a fractional frequency instability contribution from vibrations of  $<4 \times 10^{-16}$  at 1s.

To reduce temperature drifts, the resonator was thermally isolated. Two heat shields provide passive temperature stability and the outer heat shield was actively regulated by four peltier elements. The mounting and the heat shields are shown in [26]. The zero crossing of the resonator's coefficient of thermal expansion was measured to be at  $28.5(1.0)^\circ\text{C}$ . A 1% fluctuation at a pressure of  $2 \times 10^{-6}$  Pa at the ion pump, will cause a frequency instability of  $<1 \times 10^{-16}$ .

The 1069 nm and the 729 nm lasers are both extended cavity diode lasers. To transfer the cavity's fractional length stability to the laser's fractional frequency stability, we used a Pound-Drever-Hall (PDH) locking scheme [70–72]. The modulation frequency for the 1069 nm laser

was 12.3 MHz, applied with a wedged electro-optical modulator (EOM Qubig, PM7-NIR+w). The 729 nm laser was modulated at 12.7 MHz with a Brewster-cut EOM (Qubig, PM7-NIR+BC). We used two branches for feedback via a PID regulator: the fast signal controlled the laser diode current and the slow signal the external cavity grating angle. The optical setup is depicted in Fig. 1. Both laser beams are superposed in front of the cavity with a dichroic mirror. The light transmitted through the cavity was separated with a dichroic mirror to stabilise the transmitted optical power of each laser individually. For each wavelength, the transmitted light beam was split and two photodiodes were used to separately detect power fluctuations. One photodiode signal was used for the control circuit and the second allowed for an out-of-loop measurement.

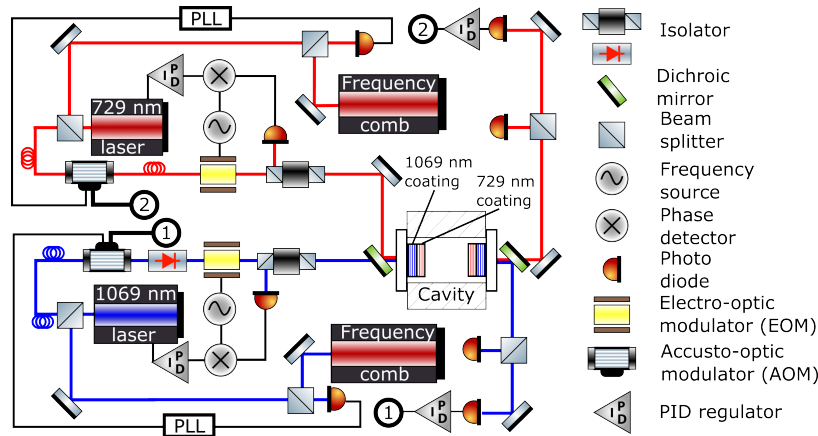


**Fig. 1.** Schematic drawing of the experimental setup. The red and the blue lines show the 729 nm laser path and 1069 nm laser path, respectively. Black lines represent electronic connections. PLL=Phase-locked loop; PID=Proportional-Integral-Derivative regulator [73]

For the frequency instability measurement, both laser frequencies were compared to a stable reference laser via an optical frequency comb. The comb was locked to a 1542 nm laser with a fractional frequency instability of  $4 \times 10^{-17}$  at 1 s [10]. Applying a transfer beat [74,75] we measured the instability of both lasers using a synchronous frequency counter in lambda counting mode [76]. By transfer locking both lasers to the frequency comb [75] via a phase-locked loop, we were able to extract frequency and phase shifts from the error signal.

### 3. Measurement and results

#### 3.1. Photo-thermal effect

Changes in the cavity resonance frequency can be caused by light power fluctuations. This is known as the photo-thermal effect [24,52,53,55–57]. The absorption of light increases the temperature in coating and substrate, causing thermal expansion. This process results in photo-thermal elastic (PTE) noise. Temperature changes can also affect the refractive index of the coating, altering the optical-path length and thus the resonance condition [54]. This process results in photo-thermal refractive (PTR) noise. In a dual-wavelength setup, both light beams are partially absorbed in the mirror coating. Thus, power fluctuations of both affect the cavity's resonances. We assume that the modulation of laser light power is slower than the heat exchange between all coating layers [58]. This means that the coating layer temperature along the beam propagation direction is time independent, and that the power absorption of both lasers will cause the same optical length change for equal amounts of dissipated power.

The theory of photo-thermal noise (PTN) for Bragg mirrors was first described in [79]. Here, we use the equations given in the supplement. Based on the material parameters (see Table 1),

the optical length change  $X$  caused by light power fluctuations can be calculated for a given mirror. The total length change  $X$  is caused by the PTR effect of the mirror coating  $X_{\text{PTR}}^{(\text{ct})}$ , the PTE effect of the mirror coating  $X_{\text{PTE}}^{(\text{ct})}$ , and the PTE effect of the mirror substrate  $X_{\text{PTE}}^{(\text{sb})}$ . The total length change  $X$  is a complex number whose absolute value  $|X|$  can be interpreted as the mirror displacement and  $\arg(X)$  is the phase between the absorbed power change and the length change. Thus, a change of phase by  $180^\circ$  changes the sign of  $X$ . The overall shift is then calculated by adding all three contributions:

$$|X| = |X_{\text{PTR}}^{(\text{ct})} + X_{\text{PTE}}^{(\text{ct})} + X_{\text{PTE}}^{(\text{sb})}|. \quad (1)$$

Since the PTE effect and PTR effect may be out of phase, it is possible to have a coherent cancellation between the three parts. The formulas can be used to design a coating with coherent cancellation between the PTR and PTE effect as shown in [80] to reduce PTN for a certain frequency range of the power noise spectrum.

**Table 1. Material parameters used. Here,  $\eta$  is Poisson's ratio,  $\alpha$  is the coefficient of thermal expansion,  $\kappa$  is the thermal conductivity,  $Y$  is Young's modulus,  $C$  is the specific heat per volume,  $\Phi$  is the mechanical loss factor, and  $\beta$  the thermorefractive index. The parameters are taken from [24,77,78] and references therein.**

	Nb <sub>2</sub> O <sub>5</sub>	SiO <sub>2</sub>	ULE
$\eta$	0.2	0.17	0.17
$\alpha$ (1/K)	$5.8 \times 10^{-6}$	$2.2 \times 10^{-6}$	$0 \pm 3 \times 10^{-8}$
$\kappa$ (W/[Km])	assumed: 1	1.38	1.38
$Y$ (GPa)	68	72	67.6
$C$ (MJ/[m <sup>3</sup> K])	2.71	1.64	1.7
$\Phi$	$4.6 \times 10^{-4}$	$2 \times 10^{-4}$	$1.6 \times 10^{-5}$
$\beta$ (1/K)	$1.43 \times 10^{-5}$	$8 \times 10^{-6}$	-
$n$ (1069 nm)	2.25	1.46	-
$n$ (729 nm)	2.29	1.46	-

The cavity's length sensitivity to power fluctuations can be measured by modulating the power of the laser light and hence the absorbed power. For the optical power calibration, we measured the transmitted laser light on a photodiode. We further expect that the measured power transmission through the cavity is proportional to the power circulating in the cavity and therefore to the absorbed power in the coatings. As the ratio between scattered and absorbed light is unknown, we cannot infer the absorbed power (see below). The amplitude and the phase of the laser frequency change can be extracted from the error signal of the transfer lock to the reference laser and were converted into an optical length change. This measurement was performed for power modulation frequencies from 10 mHz to 100 Hz. We investigated two cases. In the first, each laser frequency was locked to the resonator resonance frequency while the other laser was physically blocked. For the second, we locked both lasers to the resonator's respective resonance frequencies and one laser was power modulated, and then vice versa.

Let us first look at the frequency response of the 729 nm laser frequency as a function of its light power modulation. Figure 2 shows the corresponding optical length change of the resonator per transmitted power. The 729 nm laser power modulation showed no measurable difference between 1069 nm light blocked or frequency coupled to the resonator. The shown curves are fits of material parameters to account for effects such as the dependence on coating layer deposition [81] or the use of substrate [82]. We therefore use combination of material parameters as free parameters, i.e.  $P_{\text{abs/trans}} \times \alpha_{\text{ct}}$ ,  $P_{\text{abs/trans}} \times \beta_{\text{ct}}$ ,  $C_{\text{ct}}$ ,  $\kappa_{\text{ct}}$  and  $P_{\text{abs/trans}} \times \alpha_{\text{sb}}$ . Here,  $P_{\text{abs/trans}}$  is

the unknown scaling factor between transmission and absorption. As this is a fully correlated parameter, it cannot be determined by a fit independent from the material parameters. We fitted the data to the 1069 nm PTN sensitivity and 729 nm PTN sensitivity simultaneously, because the material parameters are the same in both cases. The fit parameters are shown in Table 2. The fitted curves of the substrate show that it does not contribute much to the 729 nm PTN sensitivity due to its low coefficient of thermal expansion (CTE). The expansion of the coating is the dominant contribution to the 729 nm laser frequency change. Most of the 729 nm power is reflected in the first layers, so that the 1069 nm stack does not make a significant contribution to the PTR noise.

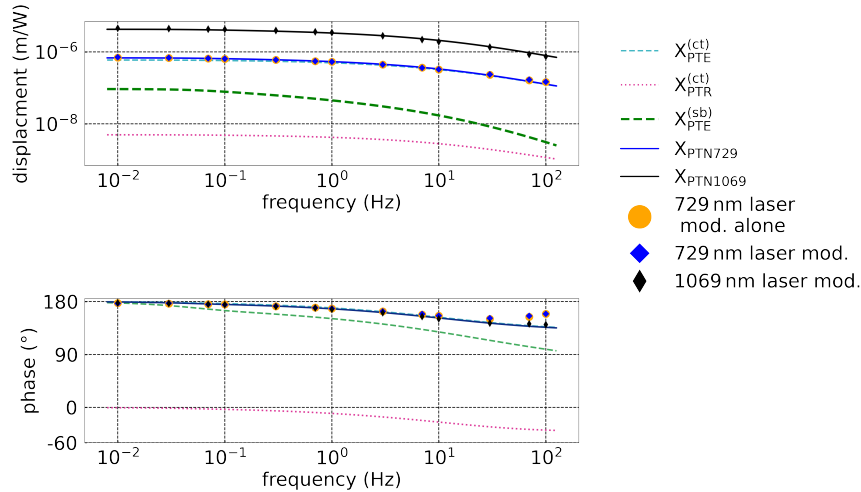


**Fig. 2.** Evaluation of the 729 nm laser frequency PTN sensitivity with theory fit to the measurement data. The upper figure shows the sensitivity and the lower one shows the phase relation. The laser modulated in power during the measurement is indicated by "mod.". The "alone" indicates that the 1069 nm laser was blocked. The shown measurement points are the average of three different power modulation settings. The contributions to the overall 729 nm PTN curves are shown for the 729 nm power modulation case with fitted material parameters. The difference in measured displacement between both lasers is due to the normalisation per transmitted power.

**Table 2.** Summary of expected material values from the literature and the material values we obtained from the fits in Fig. 2 and 3. The expected values were calculated using the values in Table 1 and the equations shown in the supplement.  $\beta_{ct}^{729}$  was not fitted because the measurement is not sensitive to the thermorefractive noise of the 729 nm coating.  $\beta_{ct}^{1069}$  and  $\beta_{ct}^{729}$  were calculated using the thin-film transfer matrix method described in [83–85].

	Literature		Fit
$\alpha_{ct}$ (1/K)	$3.6 \times 10^{-6}$	$P_{abs/trans} \times \alpha_{ct}$ (1/K)	$1.80(10) \times 10^{-5}$
$\alpha_{sb}$ (1/K)	$\pm 3 \times 10^{-8}$	$P_{abs/trans} \times \alpha_{sb}$ (1/K)	$1.2(4) \times 10^{-7}$
$\kappa_{ct}$ (W/[Km])	1.2	$\kappa_{ct}$ (W/[Km])	1.04(10)
$C_{ct}$ (MJ/[m <sup>3</sup> K])	2.1	$C_{ct}$ (MJ/[m <sup>3</sup> K])	1.37(16)
$\beta_{ct}^{729}$ (1/K)	$3.2 \times 10^{-6}$	$P_{abs/trans} \times \beta_{ct}^{729}$ (1/K)	not fitted
$\beta_{ct}^{1069}$ (1/K)	$1.54 \times 10^{-4}$	$P_{abs/trans} \times \beta_{ct}^{1069}$ (1/K)	$3.02(10) \times 10^{-4}$

Next we measured the effect of a power modulation of the 1069 nm laser light on the frequency response of the 729 nm laser frequency sensitivity, which is also depicted in Fig. 2. The length change caused by 1069 nm laser light is higher compared to the previous case because of the higher absorption. This absorption increase is due to 1069 nm light passing through the 729 nm coating layers, which absorb a certain portion of the light. We assume that the heat transfer in the coating in axial direction is faster than the laser power modulation, and that the only difference in PTN sensitivity for the 729 nm laser frequency is due to the amount of absorption and transmission differences between both lasers. As we scale to transmitted power, we do not account for this constant difference due to absorption and transmission. Therefore, we multiplied a constant absorption-to-transmission-ratio factor of  $\approx 6.2$  to the theory prediction fit of the 729 nm laser. This factor was calculated by the mean of the ratio of the 1069 nm and 729 nm laser power modulation data from Fig. 2. By using this rescaling we can fit all 729 nm and 1069 nm results with the same fit parameters. The frequency and phase behaviour due to 1069 nm power modulation is similar to the 729 nm power modulation case. So the absorption of light in lower layers of the coating does not change the PTN for the 729 nm laser.

The 1069 nm laser frequency sensitivity due to a modulation of optical laser power is shown in Fig. 3. Comparing Fig. 3 to Fig. 2, one can see that the 1069 nm PTN sensitivity is two orders of magnitude lower than the 729 nm PTN sensitivity. This is the case for power modulation by the 729 nm and 1069 nm laser. The PTE and PTR effect are out of phase and the amplitude of both effects is nearly identical. This leads to a coherent cancellation. While the refractive index change of the 729 nm stack has an impact on the optical path length of the 1069 nm light, the 1069 nm stack has no impact on the optical path length of the 729 nm light because the 1069 nm stack is positioned behind the 729 nm stack. Thus, the PTR contribution to the 1069 nm laser's frequency (Fig. 3) change is much larger compared to that of the 729 nm laser (Fig. 2) at the same light power modulation. The use of the transfer matrix approach implies that the amount of PTE noise is the same in both cases.

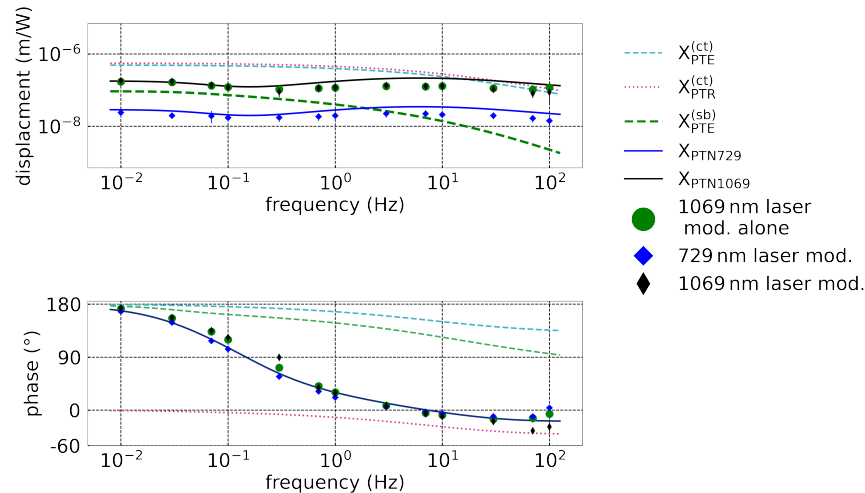


**Fig. 3.** Evaluation of the 1069 nm laser frequency PTN sensitivity with fit to measurement data. The upper figure shows the optical length change measured with the 1069 nm laser, while the lower figure shows the phase relation. The contributions to the overall 1069 nm displacement curves are shown for the 729 nm power modulation case with fitted material parameters. The shown measurement points are the average of three different power modulation settings.

Using the fit results together with measurements of the absorption, loss and transmittance of the cavity, one can derive lower bounds for the material parameters. The loss of the 729 nm cavity is 39(1) ppm and its transmission 23(1) ppm measured in only one direction. Our measurements also showed that the 1069 nm cavity has a loss of 39(3) ppm and a transmission of 11(3) ppm. To obtain the lower boundaries of the material parameters, we assume that all losses for the 1069 nm laser light are absorption losses (no scattering loss) such that  $P_{\text{abs/trans}}^{729} < 0.59$ , which gives us  $\alpha_{\text{ct}}^{\text{meas}} > 3.06(17) \times 10^{-5}$  1/K,  $\alpha_{\text{sb}}^{\text{meas}} > 2.0(7) \times 10^{-7}$  1/K, and  $\beta_{\text{ct}}^{1069,\text{meas}} > 5.11(17) \times 10^{-5}$ . For  $\alpha_{\text{ct}}$ , the measured value is one order of magnitude larger than the literature value (see Table 2). This deviation can be contributed to a low  $\alpha_{\text{ct}}^{\text{SiO}_2}$  value. As discussed in [82,85] the measured values between the bulk material or a thin film can differ because of microstructure, interface, and the underlying substrate. For the thermal expansion of Nb<sub>2</sub>O<sub>5</sub>, the reported literature values for  $\alpha_{\text{ct}}^{\text{Nb}_2\text{O}_5}$  vary from  $-2 \times 10^{-6}$  1/K to  $5.8 \times 10^{-6}$  1/K [82,86,87]. The thermal refractive index  $\beta_{\text{ct}}^{1069}$  is also higher than the literature value (see Table 2) due to the larger CTE. The thermal expansion of the substrate  $\alpha_{\text{sb}}$  is higher than expected for ULE material. The mirrors and the spacer are of the same kind of ULE glass (not the same batch), so the mirrors are operated close to the thermal zero crossing. The large discrepancy is most likely due to the low sensitivity of the fit to the substrate's thermal expansion. The fitted material parameters indeed changed by no more than  $2\sigma$  when  $\alpha_{\text{sb}}^{\text{meas}}$  was set equal to the upper end of the literature value of  $3.0 \times 10^{-8}$  1/K. The heat capacitance values exhibit a large spread as is known from the literature [77]. Our value differs by at least  $3\sigma$  compared to the closest literature value. For the thermal conductance, our value is in agreement with the literature value (see Table 2).

With the PTN sensitivity determined in Fig. 2 and 3, we can estimate the laser frequency fluctuations due to laser power fluctuations in the resonator. Fig. 4 shows that the frequency instability for the 1069 nm and the 729 nm laser is not limited by PTN. For the measurement, both lasers are power stabilised using photodiodes behind the cavity. Two additional out-of-loop photodiodes measure the remaining power fluctuations of the light transmitted through the cavity. The PTN of both cavities, 729 nm and 1069 nm, is mainly limited by the power fluctuations of the 1069 nm laser, which can be explained by the larger absorption-to-transmission ratio for the 1069 nm light compared to 729 nm light.

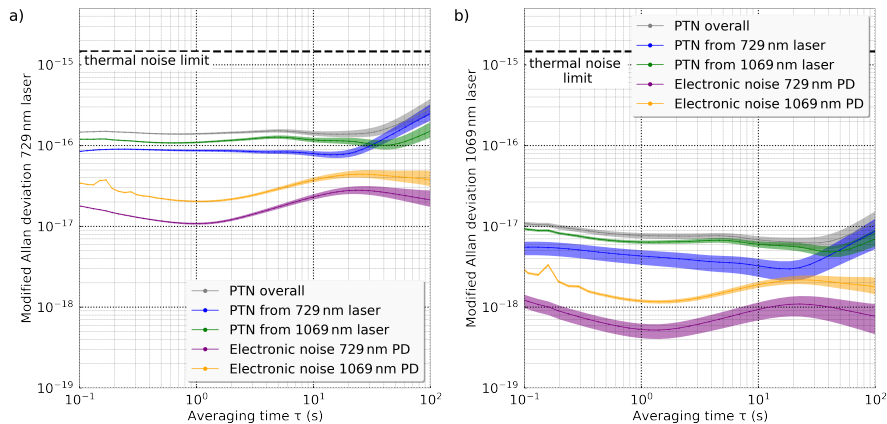


**Fig. 4.** Evaluation of fractional frequency instability due to the PTN of each laser. Figure a) [b]) shows the PTN for the 729 nm [1069 nm] laser. Both have a PTN below the thermal noise limit of the cavity. For reference, the electronic noise of the photodiodes is also shown.

### 3.2. Residual amplitude modulation (RAM)

In the PDH lock the laser light needs to be phase modulated with a fixed frequency. The demodulation of the reflected light of the cavity converts laser frequency fluctuations into amplitude fluctuations of an electronic signal. Additional optical amplitude fluctuations at the modulation frequency are called RAM and result in an offset of the electronic error signal that can change with time and thus compromise the frequency stability of the laser. One cause of RAM is birefringence in the EOM [60,61]. Another cause is that parasitic etalons affect the light amplitude of the carrier and sidebands differently [59,62]. There are stabilisation schemes which can mitigate the effect of RAM [62,88–93].

We investigated the fractional frequency instability added by RAM for two cases. First, we showed the fractional frequency instability caused by RAM for each laser by physically blocking the light of the other laser. Second, we stabilised both lasers to the cavity to observe cross-correlations which might increase the amount of RAM compared to the first case.

We measured RAM using a method similar to the one described in [24]. For this, we measured the laser frequency to voltage conversion (frequency discriminant) by modulating the PDH error signal with a known voltage and measured the corresponding frequency change at the frequency comb while the laser was locked to the cavity. This resulted in  $\approx 60 \frac{\text{kHz}}{\text{V}}$  for both lasers. For the measurement of RAM we tuned the laser away from resonance (around 150 MHz). The voltage fluctuations were measured and multiplied by the frequency discriminant to get the frequency instability caused by RAM.

In Fig. 5 (a), (b) we see the fractional frequency instability of the 729 nm [1069 nm] laser caused by RAM. For the 729 nm laser, the instability caused by RAM is above the thermal noise limit, therefore limiting the laser's fractional frequency instability. Typically, Brewster-cut and wedged EOMs introduce less RAM compared to other EOM types [94,95]. RAM voltage fluctuations of the order of 10 ppm (see, e.g., [95]) would decrease frequency fluctuations to a level of  $10^{-15}$ . Therefore, the birefringence of the EOM is unlikely to be the reason for the high RAM. We see indications for parasitic etalons due to a correlation between error signal and the scanned laser frequency far off-resonance. This was measured using a method similar to that in [59]. We found a modulation which could be caused by an etalon with a length of 5 m. This etalon is most likely located between the acousto-optical modulator and the optical isolator, therefore including the EOM (see Fig. 1). We do not expect that the RAM differs for the different cases since both lasers are phase modulated at different frequencies, which is corroborated by the near identical frequency instability of the 729 nm laser for the two cases. The slight difference in RAM for the two 729 nm laser cases can be most likely be attributed to temperature, pressure and humidity fluctuations in the lab over the course of the day and the limited measurement time for this long etalon. The frequency instability of the 1069 nm laser with the wedged EOM is not limited by RAM. The EOM shows RAM voltage fluctuations on a level of 1.6(0.1) ppm (at 1 s). The instability caused by RAM is below the thermal noise limit for averaging times  $<10$  s. We observe a measurable difference in noise caused by RAM, whether the 729 nm laser is stabilised to the cavity, or blocked. As for the 729 nm laser, we do not find evidence for an influence of the second laser on the RAM of the 1069 nm laser.

### 3.3. Fractional frequency instability

The investigation of the laser fractional frequency instability is shown in Fig. 5. Here, the individually and simultaneously locked laser instabilities are shown. The instabilities for the 729 nm laser in both cases are nearly indistinguishable and they only separate for long averaging times  $>10$  s. The laser instability appears lower than the level expected by the amount of RAM measured (for 1 – 10 s). Typically, etalons causing RAM noise vary slowly over time for example due to changes in air temperature and other laboratory conditions. Subsequent measurements can therefore yield slightly different RAM fluctuations.



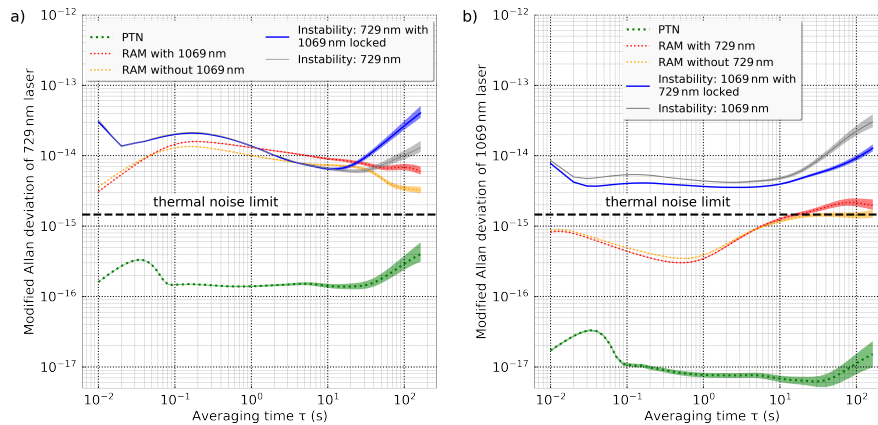


**Fig. 5.** Evaluation of the laser instability. Figure a) shows the instability of the 729 nm laser including the effects of RAM and PTN. RAM clearly limits the frequency instability of the 729 nm laser. Figure b) shows the instability of the 1069 nm laser and the effects due to RAM and PTN. All shown modified Allan deviations for laser frequency instabilities are with linear drift subtracted. All errors shown in the RAM and lasers frequency instabilities only represent the statistical error of that measurement. They do not include larger errors due to day-to-day fluctuations or measurement device errors.

For the 1069 nm laser the noise is very similar but the frequencies in the locked and unlocked cases can differ by a small amount. The difference between the measurements is limited by differential optical path length changes through optical fibres, or by small RAM fluctuations caused by the laboratory conditions changing during the experiments, and therefore differ between measurements.

#### 4. Conclusion

We investigated the possibility of achieving narrow-linewidth lasers at very different optical frequencies by locking them to the same mirror pair. The laser instability due to RAM is not correlated between the two lasers. In the case of PTN, we could see a clear correlation between frequency shift and power modulation. The light absorption of both lasers contributes to the PTN of each laser. The effect of PTN on the fractional frequency instability of the 729 nm laser is below  $2 \times 10^{-16}$  (1 s) and thus smaller than the thermal noise limit. For the fractional frequency instability of the 1069 nm laser, the PTN sensitivity was even below  $1 \times 10^{-17}$  (1 s) due to a coherent cancellation between PTR and PTE. The overall laser fractional frequency instability is  $3 \times 10^{-15}$  for the 1069 nm laser, which is around two times larger than the estimated thermal noise limit. We attributed the discrepancy to non-stabilised path lengths in the optical setup. For the 729 nm frequency lock, the fractional frequency instability was limited by RAM caused by a parasitic etalon and it only reached a level of  $1.3 \times 10^{-14}$  (1 s). This can be improved by eliminating the etalon, by finding the reflective surface, or by suppressing it using additional optical isolators. In general the thermal-noise floor and the insensitivity to RAM can be further improved by employing longer cavity spacers, thereby being able to achieve even lower length instability. In conclusion, we demonstrated that dual-wavelength coatings provide a performance similar to single-wavelength coatings in narrow-linewidth laser stabilisation and can even reduce thermal noise components through coherent cancellation.

**Funding.** Deutsche Forschungsgemeinschaft (EXC-2123 QuantumFrontiers - 390837967, SFB 1227, project B03 - 274200144, SFB 1464 TerraQ, Project-ID 434617780, and Project-ID 366146996); European Metrology Programme for

Innovation and Research; Horizon 2020 Framework Programme research and innovation programme (20FUN01 TSCAC); European Research Council (101019987); State of Lower Saxony through Niedersächsisches Vorab (QVLS-Q1).

**Acknowledgements.** The authors would like to thank Thomas Legero for the optical contacting of the cavity mirrors. We would also like to thank Uwe Sterr and Benjamin Kraus for fruitful discussions. We thank Andre Uhde and David Weber for mechanical and electrical engineering support.

**Disclosures.** The authors declare no conflicts of interest.

**Data availability.** Data underlying the results presented in this paper are not publicly available at this time but may be obtained from the authors upon reasonable request.

**Supplemental document.** See [Supplement 1](#) for supporting content.

## References

1. R. Weiss, "Nobel Lecture: LIGO and the discovery of gravitational waves I," *Rev. Mod. Phys.* **90**(4), 040501 (2018).
2. K. S. Thorne, "Nobel Lecture: LIGO and gravitational waves III," *Rev. Mod. Phys.* **90**(4), 040503 (2018).
3. B. C. Barish, "Nobel Lecture: LIGO and gravitational waves II," *Rev. Mod. Phys.* **90**(4), 040502 (2018).
4. M. Poot and H. S. J. van der Zant, "Mechanical systems in the quantum regime," *Phys. Rep.* **511**(5), 273–335 (2012).
5. D. McClelland, N. Mavalvala, Y. Chen, *et al.*, "Advanced interferometry, quantum optics and optomechanics in gravitational wave detectors," *Laser Photonics Rev.* **5**(5), 677–696 (2011).
6. M. Aspelmeyer, T. J. Kippenberg, and F. Marquardt, "Cavity optomechanics," *Rev. Mod. Phys.* **86**(4), 1391–1452 (2014).
7. C. Panuski, D. Englund, and R. Hamerly, "Fundamental Thermal Noise Limits for Optical Microcavities," *Phys. Rev. X* **10**(4), 041046 (2020).
8. L. Qiu, G. Huang, I. Shomroni, *et al.*, "Dissipative Quantum Feedback in Measurements Using a Parametrically Coupled Microcavity," *PRX Quantum* **3**(2), 020309 (2022).
9. A. D. Ludlow, M. M. Boyd, J. Ye, *et al.*, "Optical atomic clocks," *Rev. Mod. Phys.* **87**(2), 637–701 (2015).
10. D. Matei, T. Legero, S. Häfner, *et al.*, "1.5  $\mu\text{m}$  Lasers with Sub-10 mHz Linewidth," *Phys. Rev. Lett.* **118**(26), 263202 (2017).
11. W. Yam, S. Gras, and M. Evans, "Multimaterial coatings with reduced thermal noise," *Phys. Rev. D* **91**(4), 042002 (2015).
12. J. Steinlechner, I. W. Martin, J. Hough, *et al.*, "Thermal noise reduction and absorption optimization via multimaterial coatings," *Phys. Rev. D* **91**(4), 042001 (2015).
13. H. Kimble, B. Lev, and J. Ye, "Optical Interferometers with Reduced Sensitivity to Thermal Noise," *Phys. Rev. Lett.* **101**(26), 260602 (2008).
14. T. Hong, H. Yang, E. K. Gustafson, *et al.*, "Brownian thermal noise in multilayer coated mirrors," *Phys. Rev. D* **87**(8), 082001 (2013).
15. S. C. Tait, J. Steinlechner, M. M. Kinley-Hanlon, *et al.*, "Demonstration of the Multimaterial Coating Concept to Reduce Thermal Noise in Gravitational-Wave Detectors," *Phys. Rev. Lett.* **125**(1), 011102 (2020).
16. S. Hannig, L. Pelzer, N. Scharnhorst, *et al.*, "Towards a transportable aluminium ion quantum logic optical clock," *Rev. Sci. Instrum.* **90**(5), 053204 (2019).
17. S. Koller, J. Grotti, S. Vogt, *et al.*, "Transportable Optical Lattice Clock with  $7 \times 10^{-17}$  Uncertainty," *Phys. Rev. Lett.* **118**(7), 073601 (2017).
18. N. Ohmae, M. Takamoto, Y. Takahashi, *et al.*, "Transportable Strontium Optical Lattice Clocks Operated Outside Laboratory at the Level of 10-18 Uncertainty," *Adv. Quantum Technol.* **4**(8), 2100015 (2021).
19. N. Poli, M. Schioppo, S. Vogt, *et al.*, "A transportable strontium optical lattice clock," *Applied Physics B* pp. 1–10 (2014).
20. M. Zeng, Y. Huang, B. Zhang, *et al.*, "Toward a Transportable  $\text{Ca}^+$  Optical Clock with a Systematic Uncertainty of  $4.8 \times 10^{-18}$ ," *Phys. Rev. Appl.* **19**(6), 064004 (2023).
21. J. Cao, P. Zhang, J. Shang, *et al.*, "A compact, transportable single-ion optical clock with  $7.8 \times 10^{-17}$  systematic uncertainty," *Appl. Phys. B* **123**(4), 112 (2017).
22. S. Origlia, M. S. Pramod, S. Schiller, *et al.*, "Towards an optical clock for space: Compact, high-performance optical lattice clock based on bosonic atoms," *Phys. Rev. A* **98**(5), 053443 (2018).
23. J. Grotti, S. Koller, S. Vogt, *et al.*, "Geodesy and metrology with a transportable optical clock," *Nat. Phys.* **14**(5), 437–441 (2018).
24. S. Herbers, S. Häfner, S. Häfner, *et al.*, "Transportable clock laser system with an instability of  $1.6 \times 10^{-16}$ ," *Opt. Lett.* **47**(20), 5441–5444 (2022).
25. M. Pitkin, S. Reid, S. Rowan, *et al.*, "Gravitational Wave Detection by Interferometry (Ground and Space)," *Living Rev. Relativ.* **14**(1), 5 (2011).
26. S. Häfner, "Ultra-stabile Lasersysteme für Weltraum- und Bodenanwendungen," PhD Thesis, Leibniz Universität Hannover, Hannover (2015).
27. B. Argence, E. Prevost, T. Lévêque, *et al.*, "Prototype of an ultra-stable optical cavity for space applications," *Opt. Express* **20**(23), 25409–25420 (2012).

28. J. Sanjuan, K. Abich, M. Gohlke, *et al.*, “Long-term stable optical cavity for special relativity tests in space,” *Opt. Express* **27**(25), 36206 (2019).
29. C. D. Bruzewicz, R. McConnell, J. Stuart, *et al.*, “Dual-species, multi-qubit logic primitives for Ca+/Sr+ trapped-ion crystals,” *npj Quantum Inf.* **5**(1), 102 (2019).
30. M. Guggemos, D. Heinrich, O. A. Herrera-Sancho, *et al.*, “Sympathetic cooling and detection of a hot trapped ion by a cold one,” *New J. Phys.* **17**(10), 103001 (2015).
31. K.-f. Cui, J.-j. Shang, and S.-j. Chao, “Sympathetic sideband cooling of a  $^{40}\text{Ca}^+ \text{-} ^{27}\text{Al}^+$  pair toward a quantum logic clock,” *J. Phys. B: At. Mol. Opt. Phys.* **51**(4), 045502 (2018).
32. U. Tanaka, T. Kitanaka, K. Hayasaka, *et al.*, “Sideband cooling of a  $\text{Ca}^+ \text{-} \text{In}^+$  ion chain toward the quantum logic spectroscopy of  $\text{In}^+$ ,” *Appl. Phys. B* **121**(2), 147–153 (2015).
33. R. Rugango, J. E. Goeders, T. H. Dixon, *et al.*, “Sympathetic cooling of molecular ion motion to the ground state,” *New J. Phys.* **17**(3), 035009 (2015).
34. P. O. Schmidt, T. Rosenband, C. Langer, *et al.*, “Spectroscopy Using Quantum Logic,” *Science* **309**(5735), 749–752 (2005).
35. Y. Lin, D. R. Leibbrandt, D. Leibfried, *et al.*, “Quantum entanglement between an atom and a molecule,” *Nature* **581**(7808), 273–277 (2020).
36. M. Guggemos, M. Guevara-Bertsch, D. Heinrich, *et al.*, “Frequency measurement of the  $^1\text{S}_0, F=5/2 - ^3\text{P}_1, F=7/2$  transition of  $^{27}\text{Al}^+$  via quantum logic spectroscopy with  $^{40}\text{Ca}^+$ ,” *New J. Phys.* **21**(10), 103003 (2019).
37. S.-J. Chao, K.-F. Cui, S.-M. Wang, *et al.*, “Observation of  $^1\text{S}_0 \rightarrow ^3\text{P}_0$  Transition of a  $^{40}\text{Ca}^+ \text{-} ^{27}\text{Al}^+$  Quantum Logic Clock,” *Chinese Phys. Lett.* **36**(12), 120601 (2019).
38. G. Milani, B. Rauf, P. Barbieri, *et al.*, “Multiple wavelength stabilization on a single optical cavity using the offset sideband locking technique,” *Opt. Lett.* **42**(10), 1970–1973 (2017).
39. S. Wang, J. Cao, J. Yuan, *et al.*, “Integrated multiple wavelength stabilization on a multi-channel cavity for a transportable optical clock,” *Opt. Express* **28**(8), 11852 (2020).
40. I. R. Hill, R. J. Hendricks, S. Donnellan, *et al.*, “Dual-axis cubic cavity for drift-compensated multi-wavelength laser stabilisation,” *Opt. Express* **29**(22), 36758–36768 (2021).
41. F. Rohde, M. Almendros, C. Schuck, *et al.*, “A diode laser stabilization scheme for  $^{40}\text{Ca} +$  single-ion spectroscopy,” *J. Phys. B: At., Mol. Opt. Phys.* **43**(11), 115401 (2010).
42. T. Leopold, L. Schmöger, S. Feuchtenbeiner, *et al.*, “A tunable low-drift laser stabilized to an atomic reference,” *Appl. Phys. B* **122**(9), 236 (2016).
43. S. Subhankar, A. Restelli, Y. Wang, *et al.*, “Microcontroller based scanning transfer cavity lock for long-term laser frequency stabilization,” *Rev. Sci. Instrum.* **90**(4), 043115 (2019).
44. Y. Yin, Y. Xia, X. Li, *et al.*, “Narrow-linewidth and stable-frequency light source for laser cooling of magnesium fluoride molecules,” *Appl. Phys. Express* **8**(9), 092701 (2015).
45. D. P. Dai, Y. Xia, Y. N. Yin, *et al.*, “A linewidth-narrowed and frequency-stabilized dye laser for application in laser cooling of molecules,” *Opt. Express* **22**(23), 28645 (2014).
46. S. Albrecht, S. Altenburg, C. Siegel, *et al.*, “A laser system for the spectroscopy of highly charged bismuth ions,” *Appl. Phys. B* **107**(4), 1069–1074 (2012).
47. S. Uetake, K. Matsubara, H. Ito, *et al.*, “Frequency stability measurement of a transfer-cavity-stabilized diode laser by using an optical frequency comb,” *Appl. Phys. B* **97**(2), 413–419 (2009).
48. P. Bohlouli-Zanjani, K. Afrousheh, and J. D. D. Martin, “Optical transfer cavity stabilization using current-modulated injection-locked diode lasers,” *Rev. Sci. Instrum.* **77**(9), 093105 (2006).
49. P. Kruk, A. Noga, T. Trepka, *et al.*, “Frequency reference for laser spectroscopy with the stabilized 4-m-long Fabry-Perot cavity,” *Rev. Sci. Instrum.* **76**(3), 033109 (2005).
50. A. Rossi, V. Biancalana, B. Mai, *et al.*, “Long-term drift laser frequency stabilization using purely optical reference,” *Rev. Sci. Instrum.* **73**(7), 2544–2548 (2002).
51. E. Riedle, S. H. Ashworth, J. T. F. Jr, *et al.*, “Stabilization and precise calibration of a continuous-wave difference frequency spectrometer by use of a simple transfer cavity,” *Rev. Sci. Instrum.* **65**(1), 42–48 (1994).
52. K. An, B. A. Sones, C. Fang-Yen, *et al.*, “Optical bistability induced by mirror absorption: measurement of absorption coefficients at the sub-ppm level,” *Opt. Lett.* **22**(18), 1433 (1997).
53. M. De Rosa, L. Conti, M. Cerdonio, *et al.*, “Experimental Measurement of the Dynamic Photothermal Effect in Fabry-Perot Cavities for Gravitational Wave Detectors,” *Phys. Rev. Lett.* **89**(23), 237402 (2002).
54. V. Braginsky, M. Gorodetsky, and S. Vyatchanin, “Thermo-refractive noise in gravitational wave antennae,” *Phys. Lett. A* **271**(5-6), 303–307 (2000).
55. E. D. Black, I. S. Grudinin, S. R. Rao, *et al.*, “Enhanced photothermal displacement spectroscopy for thin-film characterization using a Fabry-Perot resonator,” *J. Appl. Phys.* **95**(12), 7655–7659 (2004).
56. M. D. Rosa, F. Marin, F. Marino, *et al.*, “Experimental investigation of dynamic photo-thermal effect,” *Classical Quantum Gravity* **23**(8), S259–S266 (2006).
57. A. Farsi, M. Siciliani de Cumis, F. Marino, *et al.*, “Photothermal and thermo-refractive effects in high reflectivity mirrors at room and cryogenic temperature,” *J. Appl. Phys.* **111**(4), 043101 (2012).
58. M. M. Fejer, S. Rowan, G. Cagnoli, *et al.*, “Thermoelastic dissipation in inhomogeneous media: loss measurements and displacement noise in coated test masses for interferometric gravitational wave detectors,” *Phys. Rev. D* **70**(8), 082003 (2004).

59. E. A. Whittaker, M. Gehrtz, and G. C. Bjorklund, "Residual amplitude modulation in laser electro-optic phase modulation," *J. Opt. Soc. Am. B* **2**(8), 1320–1326 (1985).
60. N. C. Wong and J. L. Hall, "Servo control of amplitude modulation in frequency-modulation spectroscopy: demonstration of shot-noise-limited detection," *J. Opt. Soc. Am. B* **2**(9), 1527–1533 (1985).
61. L. Li, F. Liu, C. Wang, *et al.*, "Measurement and control of residual amplitude modulation in optical phase modulation," *Rev. Sci. Instrum.* **83**(4), 043111 (2012).
62. H. Shen, L. Li, J. Bi, *et al.*, "Systematic and quantitative analysis of residual amplitude modulation in Pound-Drever-Hall frequency stabilization," *Phys. Rev. A* **92**(6), 063809 (2015).
63. S. Webster and P. Gill, "Force-insensitive optical cavity," *Opt. Lett.* **36**(18), 3572–3574 (2011).
64. N. Akerman, N. Navon, S. Kotler, *et al.*, "Universal gate-set for trapped-ion qubits using a narrow linewidth diode laser," *New J. Phys.* **17**(11), 113060 (2015).
65. J. Labaziewicz, P. Richerme, K. R. Brown, *et al.*, "Compact, filtered diode laser system for precision spectroscopy," *Opt. Lett.* **32**(5), 572–574 (2007).
66. J. Hald and V. Ruseva, "Efficient suppression of diode-laser phase noise by optical filtering," *J. Opt. Soc. Am. B* **22**(11), 2338–2344 (2005).
67. T. Nazarova, C. Lisdat, F. Riehle, *et al.*, "Low-frequency-noise diode laser for atom interferometry," *J. Opt. Soc. Am. B* **25**(10), 1632–1638 (2008).
68. L. Krinner, L. Pelzer, N. Spethmann, *et al.*, "A low phase noise cavity transmission self-injection locked laser system for atomic physics experiments," *arXiv*, arXiv:2311.03461 (2023).
69. K. Numata, A. Kemery, and J. Camp, "Thermal-Noise Limit in the Frequency Stabilization of Lasers with Rigid Cavities," *Phys. Rev. Lett.* **93**(25), 250602 (2004).
70. E. D. Black, "An introduction to Pound-Drever-Hall laser frequency stabilization," *Am. J. Phys.* **69**(1), 79–87 (2001).
71. R. V. Pound, "Electronic Frequency Stabilization of Microwave Oscillators," *Rev. Sci. Instrum.* **17**(11), 490–505 (1946).
72. R. W. P. Drever, J. L. Hall, F. V. Kowalski, *et al.*, "Laser phase and frequency stabilization using an optical resonator," *Appl. Phys. B: Lasers Opt.* **31**(2), 97–105 (1983).
73. A. Franzen, "Component library," <http://www.gwoptics.org/ComponentLibrary/>. 2023-11-17.
74. J. Stenger, H. Schnatz, C. Tamm, *et al.*, "Ultraprecise Measurement of Optical Frequency Ratios," *Phys. Rev. Lett.* **88**(7), 073601 (2002).
75. N. Scharnhorst, J. B. Wübbena, S. Hannig, *et al.*, "High-bandwidth transfer of phase stability through a fiber frequency comb," *Opt. Express* **23**(15), 19771–19776 (2015).
76. G. Kramer and W. Klische, "Multi-channel synchronous digital phase recorder," in *Frequency Control Symposium and PDA Exhibition, 2001. Proceedings of the 2001 IEEE International*, (2001), pp. 144–151.
77. J. Franc, N. Morgado, R. Flaminio, *et al.*, "Mirror thermal noise in laser interferometer gravitational wave detectors operating at room and cryogenic temperature," *arXiv*, arXiv:0912.0107 (2009).
78. M. Polyanskiy, "Refractive index," <https://refractiveindex.info/>. 2023-11-17.
79. V. B. Braginsky, M. L. Gorodetsky, and S. P. Vyatchanin, "Thermodynamical fluctuations and photo-thermal shot noise in gravitational wave antennae," *Phys. Lett. A* **264**(1), 1–10 (1999).
80. T. Chalermsongsak, E. D. Hall, G. D. Cole, *et al.*, "Coherent cancellation of photothermal noise in GaAs/Al<sub>0.92</sub>Ga<sub>0.08</sub>As Bragg mirrors," *Metrologia* **53**(2), 860–868 (2016).
81. V. Braginsky and A. Samoilenko, "Measurements of the optical mirror coating properties," *Phys. Lett. A* **315**(3–4), 175–177 (2003).
82. E. Çetinörgü, B. Baloukas, O. Zabeida, *et al.*, "Mechanical and thermoelastic characteristics of optical thin films deposited by dual ion beam sputtering," *Appl. Opt.* **48**(23), 4536 (2009).
83. M. Born and E. Wolf, *Principles of optics: electromagnetic theory of propagation, interference and diffraction of light* (Elsevier, 2013).
84. G. R. Fowles, *Introduction to modern optics* (Courier Corporation, 1989).
85. G. H. Ogün, "Measurement of Thermo-Optic Properties of Thin Film Dielectric Coatings," Ph.D. thesis, California Institute of Technology (2012).
86. W. R. Manning, O. Hunter, F. W. Calderwood, *et al.*, "Thermal Expansion of Nb<sub>2</sub>O<sub>5</sub>," *J. Am. Ceram. Soc.* **55**(7), 342–347 (1972).
87. H. Choosuan, R. Guo, A. S. Bhalla, *et al.*, "Negative thermal expansion behavior in single crystal and ceramic of Nb<sub>2</sub>O<sub>5</sub>-based compositions," *J. Appl. Phys.* **91**(8), 5051–5054 (2002).
88. X. Shi, J. Zhang, X. Zeng, *et al.*, "Suppression of residual amplitude modulation effects in Pound-Drever-Hall locking," *Appl. Phys. B* **124**(8), 153 (2018).
89. A. E. Domínguez, W. E. O. Larcher, and C. N. Kozameh, "Fundamental residual amplitude modulation in electro-optic modulators," *arXiv*, arXiv:1710.10719 (2017).
90. M. Descampeaux, G. Feugnet, and F. Bretenaker, "New method for residual amplitude modulation control in fibered optical experiments," *Opt. Express* **29**(22), 36211–36225 (2021).
91. W. Zhang, M. J. Martin, C. Benko, *et al.*, "Reduction of residual amplitude modulation to  $1 \times 10^{-6}$  for frequency modulation and laser stabilization," *Opt. Lett.* **39**(7), 1980 (2014).

92. C. Ishibashi, J. Ye, and J. Hall, "Analysis/reduction of residual amplitude modulation in phase/frequency modulation by an EOM," in *Summaries of Papers Presented at the Quantum Electronics and Laser Science Conference*, (Opt. Soc. America, Long Beach, CA, USA, 2002), pp. 91–92.
93. J. Bi, Y. Zhi, L. Li, *et al.*, "Suppressing residual amplitude modulation to the  $10^{-7}$  level in optical phase modulation," *Appl. Opt.* **58**(3), 690–694 (2019).
94. Z. Tai, L. Yan, Y. Zhang, *et al.*, "Electro-optic modulator with ultra-low residual amplitude modulation for frequency modulation and laser stabilization," *Opt. Lett.* **41**(23), 5584 (2016).
95. Z. Li, W. Ma, W. Yang, *et al.*, "Reduction of zero baseline drift of the Pound-Drever-Hall error signal with a wedged electro-optical crystal for squeezed state generation," *Opt. Lett.* **41**(14), 3331 (2016).